SHAKE-TABLE TEST OF A 2-STOREY LOW-DAMAGE CONCRETE WALL BUILDING

Richard S. Henry[1], Ying Zhou[2], Yiqiu Lu[1], Geoffrey W. Rodgers[3], Anqi Gu[2], Kenneth J. Elwood[1], Tony Y. Yang[4]

[1]Department of Civil and Environmental Engineering, University of Auckland, Auckland, New Zealand

[2]College of Civil Engineering, Tongji University, Shanghai, China

[3]Department of Mechanical Engineering, University of Canterbury, Christchurch, New Zealand

[4]Department of Civil Engineering, University of British Columbia, Canada

Correspondence: Yiqiu Lu, 20 Symonds St Auckland Central, Auckland, New Zealand. Email: yiqiu.lu@auckland.ac.nz

The increasing need to reduce damage and downtime in modern buildings has led to the development of a low-damage design philosophy, where the earthquake loads can be resisted with damage confined to easily replaceable components. Post-tensioned concrete walls have emerged as a popular low-damage structural system that have been implemented in a range of buildings. In order to provide essential evidence to support the development of low-damage concrete structures, a system-level shake-table test was conducted on a 2-storey low-damage concrete wall building implementing state-of-art design concepts. The test building included post-tensioned (PT) rocking walls that provide the primary lateral-load resistance in both directions, a frame that utilised slotted beam connections, and a range of alternative energy dissipation devices that were installed at wall base or/and beam-column joints. The building was subjected to 39 tests with a range of intensity ground motions, incorporating both unidirectional and bi-directional ground motions on the structure with different combinations of wall strength and energy dissipating devices. The building performed exceptionally well during the intense series of tests, confirming the suitability of both the design methods and the connection detailing implemented. The building achieved an immediate occupancy performance objective even when subjected to maximum considered earthquake hazard shaking. The building exhibited only minor damage at the conclusion of testing, with distributed cracking in the floors and cosmetic spalling in the wall toes that did not compromise structural capacity or integrity and could be easily repaired with minimal disruption. The test has provided a rich dataset that is available for further analysis of the building response and validation of design methods and numerical models.

Keywords
Shake-table test, system level, low-damage design, PRESSS, seismic design, displacement-based design, precast concrete, post-tensioned wall, rocking wall, slotted beam, wall-to-floor, energy dissipating device, self-centering, repairability.

INTRODUCTION

Damage to conventionally designed modern buildings during major earthquakes can result in costly repairs or demolition, even when buildings perform as intended by the designer. For example, over 60% of multi-storey buildings that were predominantly capacity-designed reinforced concrete structures were demolished following the 2010/2011 Canterbury earthquakes in New Zealand [1]. The increasing need to reduce post-earthquake damage and downtime to modern buildings has led to the development of the low-damage design philosophy where earthquake demands can be resisted with damage confined to easily replaceable components.

A range of different low-damage technologies have been developed and implemented that are suitable for different structural systems and building types. Post-tensioned (PT) precast concrete systems that allow for jointed behaviour with a self-centering response were investigated during the PRESSS research program [2], and have been the subject of extensive research to develop alternative structural components and systems [3]. Unboned PT walls can be designed as a single rocking wall where uplift occurs at the wall base and the PT provides both strength and re-centering [4, 5]. Single rocking walls are characterised by a non-linear elastic response with minimal energy dissipation. To improve the energy dissipation capacity, unbonded PT walls can be configured with supplementary energy dissipating devices such as in hybrid wall systems that use either mild steel bars or viscous dampers [6-9], jointed wall systems [2], and the Precast Wall with End Columns (PreWEC) [10, 11]. Recent investigations of PT walls have focused on shake-table testing to quantify dynamic performance and validate seismic design provisions [12, 13].

Research into unbonded PT precast concrete systems has led to the publication of design standards and guidelines to support implementation. In New Zealand, provisions for the design of ductile jointed precast systems were introduced into an appendix of the Concrete Structures Standard (NZS 3101) in 2006 [14] and detailed design guidelines were published in by the New Zealand Concrete Society in 2010 [15]. In the US, acceptance criteria and design provisions for unbonded PT walls was published by the American Concrete Institute (ACI) [16, 17] and cited by the Building Code Requirements for Structural Concrete (ACI 318) in 2008 [18]. Early adoption of unbonded PT precast concrete utilised hybrid frame systems [19], while more recent implementation in New Zealand has predominantly utilised hybrid and coupled wall systems or dual wall-frame systems [20-22]. However, implemented buildings have often adopted structural systems and configurations that differ from those tested by researchers. In addition, published design guidelines tend to focus on the component design, leaving engineers to develop connection detailing from first principles.

With unbonded PT component design and performance well established, researchers have shifted focus to the system-level response and interaction between structural components in buildings. The behaviour of alternative wall-to-floor connections in PT wall buildings was investigated using numerical models [23] and innovative connectors have been tested that can isolate the floor from the vertical uplift of the wall while still maintaining a horizontal load path [24]. In addition, large-scale subassembly tests confirmed that significant deformations and damage are induced in floors when connected integrally with a PT wall and showed that the use of an isolated wall-to-floor connection could successfully reduce out-of-plane floor deformations to ensure a more predictable lateral-load response [25].

When considering the entire structure, two relevant shake-table tests of buildings that incorporated PT walls have previously been conducted. A four storey building that utilised hybrid PT walls in one direction was tested on the E-defense shake-table [26]. Although the PT walls performed adequately, the test highlighted the potential damage that can occur to other structural components and connections when deformation compatibly and secondary forces due to structural interactions are not adequately considered during design. Damage occurred at the wall-to-floor interface where the PT walls were monolithically connected to the topping of the precast floor units and crushing at the column bases occurred due to increased axial demands from outrigger framing action. A numerical model developed for the E-defense test building showed that the inclusion of the beams connected between the wall and columns as well as in-plane and out-of-plane response of the floors were essential to accurately capture the lateral-load response of the entire building [27]. A separate unidirectional test of a three storey precast concrete building that incorporated hybrid PT walls was completed on the shake-table at UC San Diego [28, 29]. Although the test primarily focused on the diaphragm response, the test confirmed that slotted connectors could be implemented between the wall and floor to enable horizontal force transfer while allowing unrestrained uplift of the PT walls. The design of such slotted connectors needs careful consideration to ensure appropriate robustness, with the test highlighting the potential damage that can result to the floors when the wall uplift exceeds the connector slot travel.

Despite the extensive research to support the development of low-damage structural systems, and in particular PT walls, there is a lack of guidance on the system-level design of entire buildings. Prior research into the system response has identified the potential impacts of not considering displacement compatibility between components and novel solutions have been proposed that require further testing to support adoption into engineering practice. A bi-directional shake-table test of a 2-storey full-scale PT wall building was conducted to verify the seismic response of a low-damage concrete wall building implementing state-of-art design concepts and practical construction details. The test was completed at the Tongji University multi-functional shake-table array as part of a collaborative research project between the New Zealand Centre for Earthquake Resilience (QuakeCoRE) and the International Joint Research Laboratory of Earthquake Engineering (ILEE). The results of the test building were used to assess whether current design procedures were adequate to achieve low-damage design objectives and for interactions between the structural components to be investigated when subjected to bi-directional shaking demands. The building was designed with several configurations to allow for alternative design objectives and connection detailing to be compared over a range of earthquake demands. The experimental program is outlined and the key test results are presented, focusing of the overall building response and response of key components and connections.

EXPERIMENTAL PROGRAM

The test building was designed to represent implemented low-damage concrete buildings with several configurations allowing for multiple comparisons to achieve the project objectives. A full-scale 2-storey building was designed with a floor plan and total mass of approximately 140t that equalled the limit of the pair of shake-tables used for the project. The building design was based on existing design standards and guidelines with connection detailing that was specifically recommended by a panel of structural engineers with experience in implementing such low-damage buildings. An

overview of experimental program is provided and additional details of the test building have been published on DesignSafe-CI [30].

Description of the test building

The constructed 2-storey building on the shake-table prior to testing is shown in Figure 1. The building was designed in accordance with the New Zealand Concrete Structures Standard [14] and the PRESSS Design Handbook [15] using the Direct Displacement-Based Design (DDBD) procedure [31]. The building was assumed to be used for general office purpose in a region of high seismicity, specifically Wellington, New Zealand.

Figure 1 Test building

The test building consisted of plan dimensions of 5.40 × 8.95 m and a total height of 8 m with each storey 4 m high, as shown in the plan and elevation drawings in Figure 2. The building was designed with PT precast concrete rocking walls that provided the primary lateral-load resistance in both directions and a perimeter frame that primarily resisted gravity loads but acted as a dual lateral-load resisting system for some tests. The PT walls in the longitudinal (x) or EW direction on Grids 1 and 3 had a length of 2500 mm, a thickness of 150 mm, and were constructed integral with the frame and floors with separate panels for each floor level. The PT walls in the transverse (y) or NS direction on Grids A and C had a length of 2000 mm, a thickness of 150 mm, and were constructed as a single full height panel positioned offset from the frame. Alternative detailing was used for the wall base connections in each wall, with drawings shown in Figure 3. The Grid 1 and 3 walls had light armouring consisting of a 30 mm high equal angle around the edge of the wall base and used a grouted wall-to-foundation connection with a 25 mm fibre reinforced grout layer confined in a pocket at the top of the foundation. The grouted connection relied on friction for shear transfer at the wall base with no additional shear dowels. The Grid A and C walls had heavier armouring consisting of a 40 mm high equal angle around the edge of the wall as well as additional 8 mm thick steel plates on three sides at the ends of the wall that extended 150 mm high and 250 mm along the wall. A steel pocket connection was used at the Grid A and C wall base where the wall armouring was constructed to fit a steel pocket component embedded within the foundation with angled sides (5° taper) to allow for wall rotation. In addition to friction at the wall base, the steel pocket provided an additional shear transfer mechanism when the wall armouring contacted the sides of the steel pocket. The post-tensioning tendons were designed for several design configurations, as is discussed in more details in subsequent sections.

The frames consisted of 300×400 mm perimeter beams and 400×400 mm square corner columns that were constructed as precast components. The beam-column and beam-wall joints were precast with the beams as a single component and connected to the column or wall components with grouted reinforcement connections. The beams were precast as half-beams with the top portion cast at the same time as the in-situ floor topping and an in-situ concrete stitch at mid-span. In order for the frame to meet the low-damage design objective, the column base used a rocking connection and the beams utilised a non-tearing slotted beam connection, as developed by Bull et al. [32]. A slot constructed in the beam adjacent to the column or wall face allows rotation demands to be accommodated by opening and closing of the slot with a centre of rotation at the top of the beam to minimise axial elongation demands on the floors. Beam shear and torsion was resisted by diagonal hanger reinforcement installed between the column and beam. The slotted beams acted as pinned connections when no energy dissipating devices were installed or as moment resisting connection when energy dissipating devices were installed across the bottom of the beam slot. An example of a slotted beam joint with energy dissipating devices installed is shown in Figure 3. The column base connection was designed to act as a pin and were armoured with 50 mm high equal angles and used a grouted base connection. An unstressed PT bar located at the centre of the level 1 column to resist potential column tension demands during earthquakes.

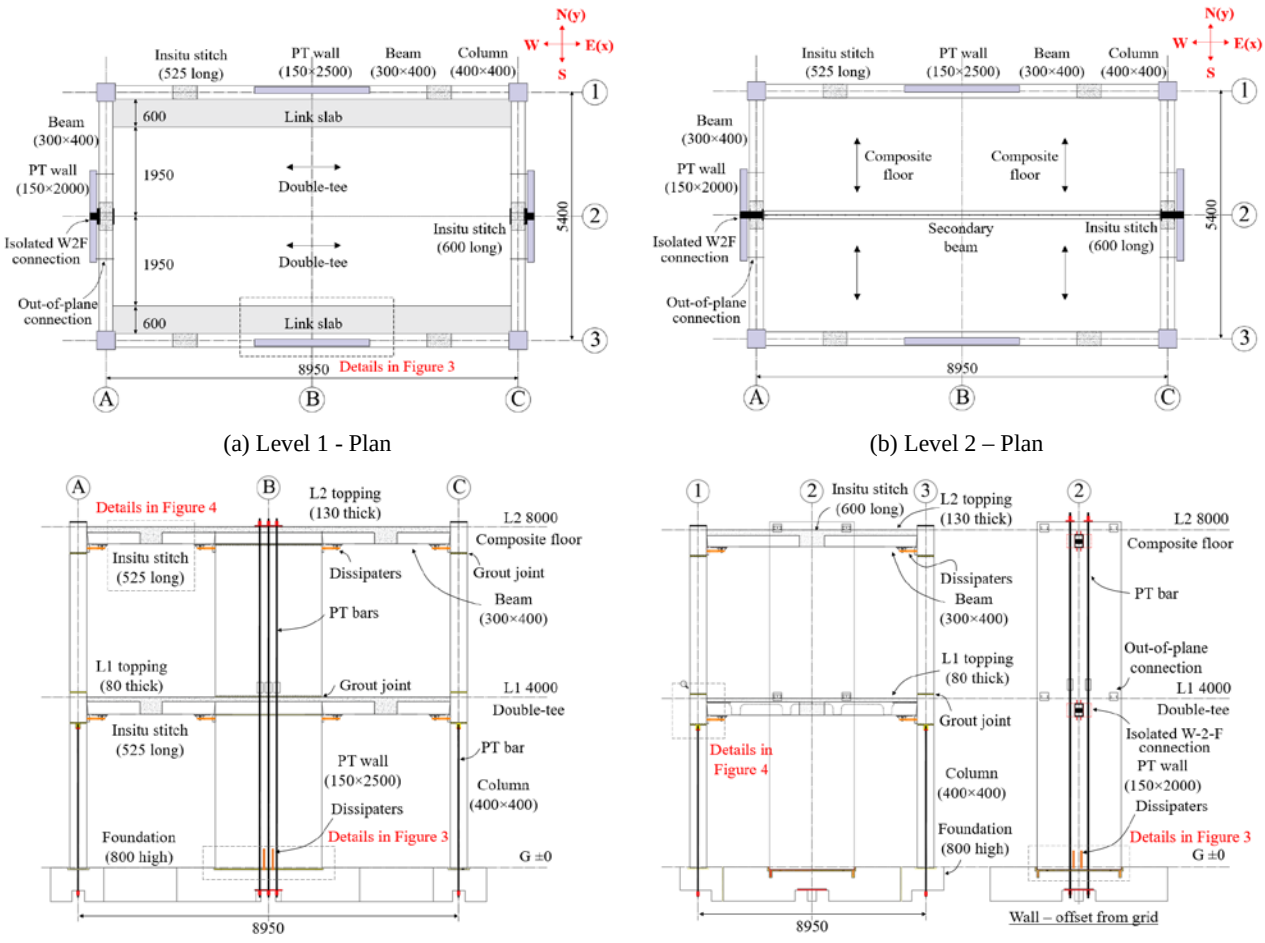

(a) Level 1 - Plan

(b) Level 2 – Plan

(c) Grid 1/3 – Elevation

(d) Grid A/C – Elevation

Figure 2 Building floor plan and elevations

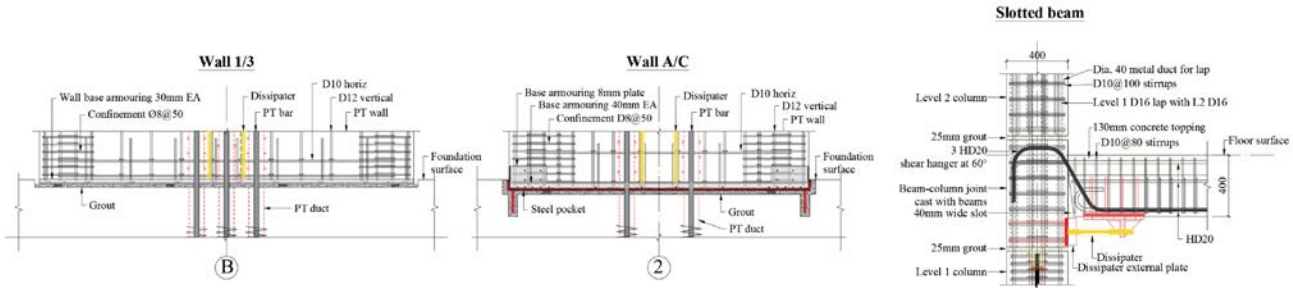

Figure 3 Wall base detailing

Two different floor systems were used in the test building, as shown in Figure 2. The level 1 floor consisted of long-span 300 mm deep precast concrete double-tee units with an 80 mm in-situ concrete topping. The double-tees used an armoured flange hung support detail that allowed them to pivot about the topping similar to the slotted beams. A steel tray composite floor (ComFlor 60) was used for the level 2 floor in a short span configuration with steel decking as permanent formwork and a 130 mm thick concrete slab. A secondary steel beam was positioned through the center of the level 2 floor plan to reduce the span of the composite floor. Two alternative wall-to-floor connection designs were implemented to accommodate the potential displacement incompatibility as the walls uplifted, with drawings shown in Figure 4. A flexible wall-to-floor connection was used for the Grid 1 and 3 walls in the longitudinal direction that were designed to be sufficiently stiff to transfer in-plane diaphragm loads while being flexible in the out-of-plane direction to accommodate wall uplift and rotation. On Level 2, the composite floor provided sufficient flexibility when spanning perpendicular to the wall, and on Level 1 a 600 mm wide and 80 mm thick link slab was located between the wall and the first double-tee

unit. Isolated wall-to-floor connections were used for the Grid A and C walls in the transverse direction with the configuration of the frames such that the wall was not required to resist gravity loads from the floors. A steel tongue that was embedded in the beam extended out into an armoured slot that was cast in the wall panels. The tongue allowed for lateral force transfer to the PT wall in bearing but was free to slide vertically with sufficient travel for demands exceeding maximum consider earthquake demands. An initial 10 mm gap was designed into the steel tongue connection for tolerance that was later filled with high density plastic shims. The steel tongue only provided an in-plane connection and so additional pinned struts were used to provide an out-of-plane connection at the ends of the wall on both floor levels.

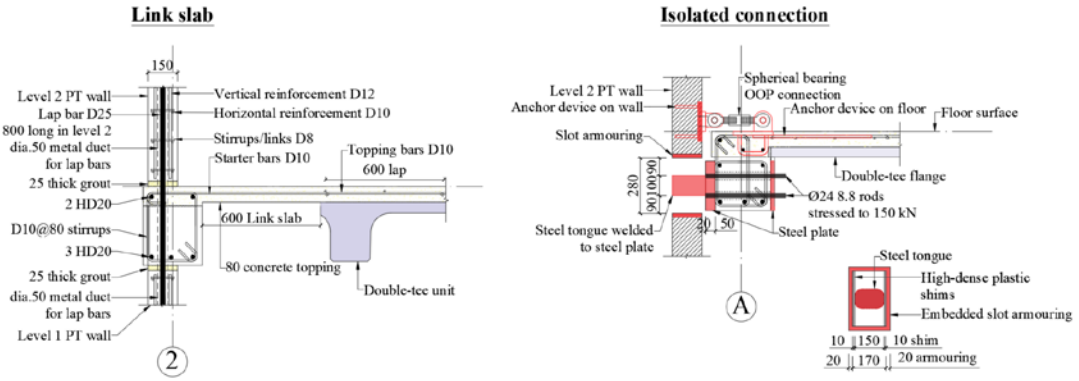

Figure 4 Wall-to-floor connections

Additional mass of 72.2 kN per level was used to simulate the superimposed dead and live loads for the test building. The additional mass consisted of steel and lead mass blocks that were distributed throughout the floor plan, consisting of blocks stacked and glued around the perimeter beams using a high bond strength silicon sealant and 12 steel boxes filled with blocks bolted to the floor on each level. The blocks initial position was marked prior to testing and inspections of the blocks between tests confirmed that they had not moved and remained securely fixed to the floor. The total seismic weights of the test building including self-weight and added mass were equivalent to 522 kN and 357 kN for level 1 and level 2, respectively.

Design configurations

The building was designed to compare a range of design objectives and configurations. Due to the low-damage nature of the building, a large number of tests could be performed on the building with only key components modified or replaced between configurations. The building was designed for three lateral drift targets using different combinations of wall strength and energy dissipating devices, as summarised in Table 1. For Design 1 the lateral drift target of 1% represented a design where drifts are limited to prevent damage to non-structural components and required the largest equivalent viscous damping of 11%. Three combinations of energy dissipating devices were used at either the wall base of beam-column joints in Design 1, including steel fuse groove-type dissipaters [33], high force-to-volume (HF2V) lead-extrusion dampers [34] and viscous fluid dampers [35]. The three combinations of energy dissipating devices were intended to achieve comparable strength and energy dissipation, resulting in Design 1a, 1b and 1c. For Design 2, a higher lateral drift target of 2% was achieved with lower 5% target equivalent viscous damping, with the drifts comparable to implemented ductile buildings. For Design 2 only steel fuse dissipaters were installed at the wall base, and these dissipaters were designed for a lower yield force and higher displacement demand than the steel fuses used in the same location in Designs 1a and 1c. For Design 3, no energy dissipating devices were installed in the test building, representing a PT system relying on inherent viscous and impact damping only, and was intended to test the resilience of the system when energy dissipating devices had failed. Additional torsional design configurations were included in the test program and will be reported separately.

For each design case, the wall PT bar area, initial PT stress, and the strength of the energy dissipating devices in both the wall base and slotted beam joints were designed based on an iterative process to meet the following key design criteria:

- Required building lateral capacity at the design drift, calculated from the DDBD [31] seismic analysis.
- Equivalent viscous damping assumed for the building design.
- For Design 1, the dual system was designed targeting ~80% of the lateral strength provided by the PT walls and ~20% provided by the slotted beams.
- PT bar stresses at the design drift not exceeding $0.9f_{py}$ (as per New Zealand Concrete Structures Standard [14]).

Table 1 Building design configurations

Design	Design drift	ξ	Dissipating devices		PT		Design action		λ	
			Wall base	Beam joint	Wall 1/3	Wall A/C	M_b (kNm)	V_b (kN)	Wall 1/3	Wall A/C
D1a	1%	11%	Steel fuse	Steel fuse	1Φ25 f_{pi} = 680 MPa	2Φ25 f_{pi} = 451 MPa	1058	168	1.10	0.93
D1b	1%	11%	Viscous damper	HF2V			1058	168	1.74	1.50
D1c	1%	11%	Steel fuse	HF2V			1058	168	1.10	0.93
D2	2%	5%	Steel fuse	N/A	2Φ25 f_{pi} = 421 MPa	2Φ32 f_{pi} = 443 MPa	1145	181	6.63	6.91
D3	3%	3%	N/A				1175	186	$\propto$	$\propto$

Notes: f_{pi} = initial stress applied to the PT tendons, ξ = equivalent viscous damping ratio, M_b = building base moment, V_b = building base shear, and λ is the ratio of moment provided by PT and axial loads to the moment provided by all energy dissipating devices at design drift.

Material properties

The design specific compressive strength (f'_c) of the precast components and in-situ concrete joints was 40 MPa and was constructed using a C50 concrete mix. The floor topping had a design specific compressive strength of 30 MPa and was constructed using a C40 concrete mix. The grouted connections between precast components (e.g. panel-to-panel and column-to-column joints) used Liwubao C80 grout and C120 grout mixed with 6 mm steel fibres was used at the wall and column base. The average measured concrete and grout compressive strengths for different components at the time of testing are listed in Table 2. The measured concrete strengths all exceeded the specific concrete strengths, typically 30-50% above for precast components and 12-20% above for in-situ concrete. Two types of PT bars PSB1080-25 (PT25, diameter 25 mm) and PSB1080-32 (PT32, diameter 32 mm) were used for the PT walls and both had a specified yield strength (f_{py}) of 1080 MPa and ultimate strength (f_{pu}) of 1230 MPa. Columns used PSB785-15 PT bars (PT15, diameter 15 mm, f_{py} = 785 MPa). Reinforcement consisted of HPB300 (round bars, f_y = 300 MPa), HRB400E (deformed bars, f_y = 400 MPa) and HRB500E (deformed bars, f_y = 500 MPa). Table 2 lists the average measured yield and ultimate strengths and ultimate strains at maximum stress of all bars.

Table 2 Measured concrete and reinforcement strengths

Concrete	Location	f'_c (MPa)
Precast components C50	Foundation	60.2
	Column L1/L2	58.6/57.2
	Beam L1/L2	58.4/56.1
	Wall 1&3 / A&C	58.6/56.3
	Double-tee	52.6
Beam stitch C50	Level 1	45.8
	Level 2	45.0
Floor topping C40	Level 1	36.2
	Level 2	36.6
Grout C80	Joints	87.2
Fiber grout C120	Wall 1/3 base	131.9

Reinforcement	Location	f_y (MPa)	f_u (MPa)	ε_u (mm/mm)
PT15	Columns	849	1039	11.5%
PT25	Wall 1/3 for all designs Wall A/C for Design 1	1159	1239	4.7%
PT32	Wall A/C for Design 2&3	1137	1221	2.2%†
HD16	Beam shear hangers	5230	705	13.7%
HD20	Beam shear hangers	507	676	14.3%
	Beam longitudinal	508	663	14.6%
D16	Column longitudinal	433	616	14.4%
D12	Wall longitudinal	484	579	12.9%
D10	Wall horizontal	472	672	12.9%
	Beam stirrups	407	518	13.2%
R8	Wall confinement	333	456	11.7%

† *not loaded to failure*

Energy dissipating devices

Three types of energy dissipating devices were used for different design configurations during the test, including steel fuse dissipaters, HF2V lead-extrusion dampers, and viscous dampers. The steel fuse dissipaters used in the test were manufactured from a Grade 300E reinforcing round (reinforcing bar without deformations) that were milled to create a reduced groove-type active section where yielding was intended. A confining steel tube was positioned around the fuse to prevent buckling. Drawings and photos of an example steel fuse dissipaters used in the Grid A/C beam-column joints for Design 1 are shown in Figure 5. Table 3 lists the key target force and displacement design parameters and the cross-sectional area and length of active section of each steel fuse dissipater used in the different building design configurations. Additional test reports for the energy dissipating devices are available in the published dataset on DesignSafe-CI [30]. The HF2V and viscous dampers were designed for an equivalent response to the steel fuses and the test results for building D1b and D1c configurations that used will be published separately.

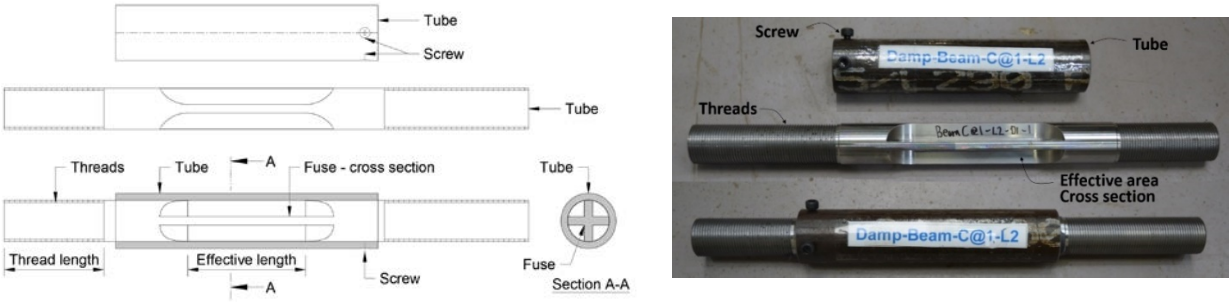

(a) Drawings (b) Photo

Figure 5 Example of steel fuse dissipater

Table 3 Design of steel fuse dissipaters

Design	Location	Grid 1/3				Grid A/C			
		A_{act} (mm^2)	L_{act} (mm)	F_d (kN)	d_d (mm)	A_{act} (mm^2)	L_{act} (mm)	F_d (kN)	d_d (mm)
D1	**Wall base**	173	165	63	9.8	220	140	83	6.9
	Slotted beam joint	173	165	61	7.4	365	90	181	4.2
D2	**Wall base**	101	410	38	20.5	142	290	50	14.5

Notes: A_{act} = cross-section area of the active section, L_{act} = length of the active section, F_d = target design force, d_d = design displacement.

Instrumentation

The test building was instrumented with a dense array of sensors consisting of a total of 360 channels of data recorded at 256 Hz to monitor the overall building response as well as local component responses. Figure 6 illustrates key instrumentation locations, where the arrangements shown applied to all floors, elevations, and components. Full instrumentation drawings and descriptions are available in published dataset on DesignSafe-CI [30].

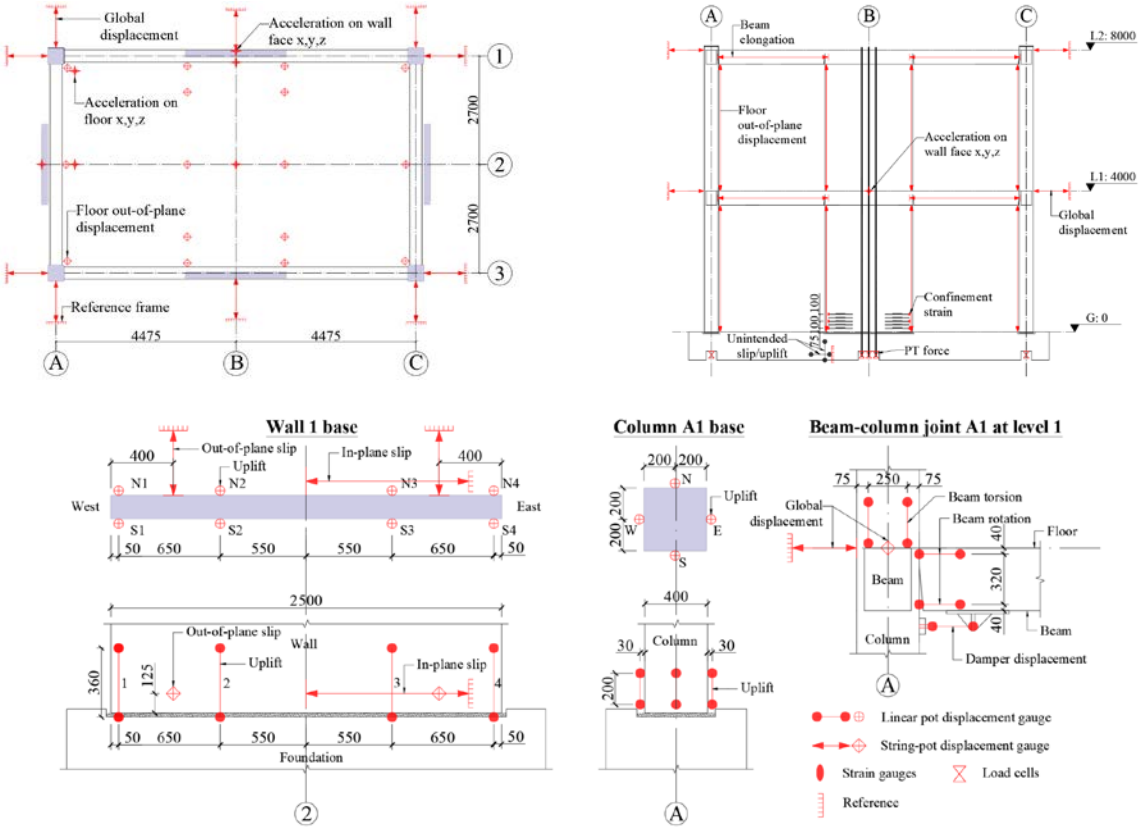

Figure 6 Instrumentation drawings

Triaxial accelerometers were placed in two corners of the foundation, four locations on each floor slab, and on one wall in each direction at the floor levels. Global building lateral displacements were measured using high tension string-pot displacement gauges (SPDG) that were mounted on a reference frame that surrounded the entire building with wires connected to the foundations, columns, and walls on all grid lines and levels. Rows of linear-pot displacement gauges (LPDG) were installed on both sides of each wall base allowing the in-plane and out-of-plane uplift profiles and base rotations to be calculated and four LPDGs were installed at the center of four faces at each column base. The slotted beam joint opening and rotations were monitored by a pair of LPDGs across the top and bottom of all beam slots. Out-of-plane floor deflections at 16 locations were measured by SPDGs extending vertically from the shake-table to the bottom of the level 1 floor and from the top of the level 1 floor to the bottom of the level 2 floor. Axial elongation of all the beams were measured by SPDGs mounted either beside or above the beam. Torsional rotations and shear slip at the beam joints were measured with a pair of LPDGs installed between the column and top of the beam for four joint locations. Unintended uplift and horizontal slip at the base of each foundation was monitored with LPDGs. SPDGs were installed at bases of all four walls to monitor both potential in-plane and out-of-plane slip at the wall-to-foundation joints. Strain gauges were attached in a number of reinforcing bars prior to concrete pouring to monitor the strain of shear hangers and top longitudinal reinforcement at three slotted beam-column joints, floor starter bars at two ends of wall 1 at each level, and confinement reinforcement at the base of wall 1 and wall A. The forces in all PT bars where measured by load cells that were installed at the PT anchor at the foundation.

Ground motions and test sequence

Ground motions were selected to represent the seismic hazard for soil class C in Wellington, New Zealand, including serviceability limit states (SLS) at 25% and 50% of design level intensity, ultimate limit state (ULS) at 100% design level intensity, and maximum consider earthquake (MCE) at 180% design level intensity. Ground motions were selected from existing datasets [36, 37] that were generally spectrum compatible over the building period range and that has similar intensity for both components. The SLS ground motion was from the 1979 Imperial Valley earthquake Parachute Test Site station (RSN-187). The ULS or design level ground motions included both a far-field and a near-fault record. The far-field (FF) record was from the 1995 Kobe earthquake, Nishi-Akashi station (RSN-1111), and the near-fault (NF) record was from the 1989 Loma Prieta earthquake, Saratoga – Aloha Ave station (RSN-802). The MCE ground motions consisted of the two ULS records with a higher scale factor as well as a long-duration ground motion record from the 1985 Chile earthquake (Chile), San Fernando station. The ground motions were scaled in accordance with NZS 1170.5 [38] over a period range from the lowest fundamental period (0.16 s) to the highest effective period (1.04 s). During unidirectional tests, the scaled principal component from the ground motion was applied (regardless of building direction tested). During bi-directional tests, the principal component was subjected to the NS (y) direction of the building and the secondary component was applied to the EW (x) direction of the building. The measured elastic 5% damped acceleration spectra of the primary component of the shake table response for various tests are compared against the target response spectra in Figure 7.

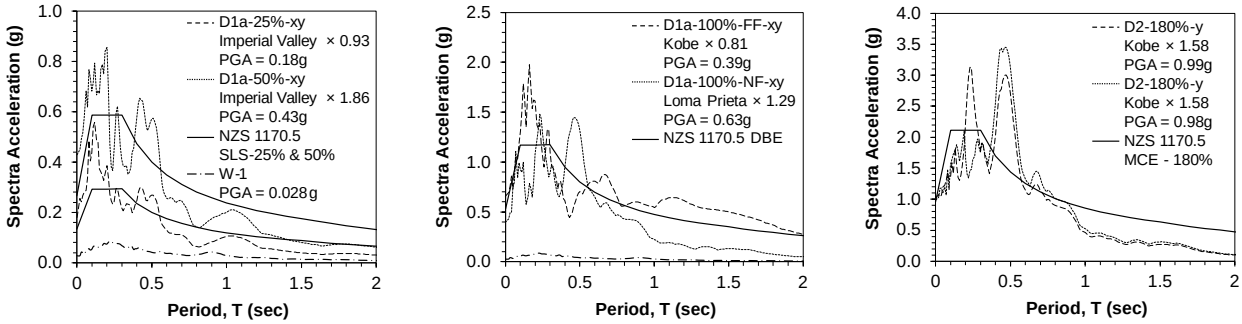

Figure 7 GM acceleration response spectra

A total of 39 tests were conducted over a 6-day period. The building was subjected to unidirectional shaking in both directions of the building followed by bi-directional shaking for most configurations and ground motion intensities. The Design 1a building was first subjected to SLS (25%), SLS2 (50%) and ULS (100%) tests, followed by ULS (100%) tests for Design 1b and 1c. The energy dissipating devices were replaced between the 1a, 1b and 1c tests as well as replacement of damaged shims in the isolated wall-to-floor connectors. Prior to Design 2, the PT bars were restressed and new energy dissipating devices were installed. The Design 2 building was subjected to ULS (100%) and MCE (180%) ground motions. The Design 2 building was subsequently modified to create deliberate strength irregularity in the walls to generate a torsional response and the results of these tests will be published separately. The final Design 3 building was subjected to ULS (100%) and close to MCE (150%) ground motions. Before and after each set of ground motions, the building was

subjected to low-amplitude white-noise excitation with PGA of ~0.03g. An example response spectra for the white noise tests is included in Figure 7 in comparison to the SLS intensity ground motions.

TEST RESULTS AND KEY FINDINGS

Global Building Response

In general, the building performed exceptionally well during the entire test sequence. Inelastic deformations were controlled by uplift and rocking at the wall and column bases and opening and closing of the slotted beam joints in accordance with the building design philosophy. The building was subjected to the entire test sequence and ground motion intensities without any structural failures occurring and without significant loss of lateral-load capacity or residual drifts at the conclusion of testing. The test building was designed close to the payload capacity of the shake-table and with the exception of the bi-directional MCE (180%) tests all ground motions were successfully completed. The table reached the overturning moment capacity limit and shutdown during the first bi-directional MCE (180%) test (D2-180%-S1-xy) and subsequent 180% intensity tests were instead completed uniaxially (both x and y directions).

A summary of the peak global response parameters recorded for the D1a, D2, and D3 tests are provided in Table 4, including peak ground and roof accelerations, peak roof drifts and residual drifts, and peak base moments and shears. Accelerations were filtered with a low pass filter with a 45 Hz cut-off frequency. Building drifts were calculated from the average of all column lateral displacements in each direction and the as-built inter-storey heights. The building base shear and moment demands were calculated from the horizontal inertia forces over each floor, with inertia forces calculated from the associated floor mass and floor accelerations measured by the B2 accelerometer positioned at the center of the floor area.

Table 4 Peak global response parameters

Test		EW (x) direction						NS (y) direction						θ (%)
		PGA (g)	PRA (g)	$d_{max,r}$ (%)	$d_{res,r}$ (%)	M_b (kN-m)	V_b (kN)	PGA (g)	PRA (g)	$d_{max,r}$ (%)	$d_{res,r}$ (%)	M_b (kN-m)	V_b (kN)	
D1a 25%	D1a-25%-x[2]	0.19	0.45	0.08	0.00	1672	267	0.03	0.03	0.01	0.00	105	20	0.02
	D1a-25%-y	0.02	0.07	0.01	0.00	239	35	0.19	0.41	0.12	0.00	1358	262	0.02
	D1a-25%-xy	0.12	0.33	0.05	0.00	1238	195	0.18	0.39	0.11	0.00	1311	253	0.02
D1a 50%	D1a-50%-x	0.32	0.59	0.11	0.00	2041	303	0.04	0.06	0.02	0.00	218	35	0.02
	D1a-50%-y	0.03	0.10	0.01	0.00	329	48	0.33	0.71	0.41	0.00	2609	443	0.03
	D1a-50%-xy	0.30	0.58	0.14	0.00	2151	332	0.43	0.77	0.44	-0.01	2552	442	0.08
D1a 100%	D1a-100%-FF-x[2]	0.48	1.03	0.63	0.00	3894	607	0.04	0.08	0.02	0.00	339	57	0.03
	D1a-100%-FF-y	0.03	0.11	0.03	0.00	343	48	0.49	1.04	1.06	-0.01	3384	545	0.03
	D1a-100%-FF-xy	0.36	0.86	0.54	0.00	3395	541	0.39	1.00	0.94	-0.01	3259	529	0.11
	D1a-100%-NF-xy[3]	0.53	0.91	0.47	0.00	3125	492	0.63	0.81	0.78	-0.01	2843	493	0.07
	D1a-25%-xy-2	0.13	0.24	0.05	0.00	833	123	0.17	0.35	0.17	-0.01	1080	205	0.03
D2 100%	D2-100%-FF-x[2]	0.48	1.18	1.29	0.00	4021	604	0.04	0.09	0.10	-0.01	267	52	0.12
	D2-100%-FF-y[2]	0.04	0.17	0.04	-0.01	595	89	0.57	0.97	1.20	-0.02	3116	496	0.09
	D2-100%-FF-xy	0.39	1.23	1.07	0.00	3109	498	0.53	1.21	1.22	-0.02	3233	500	0.18
	D2-100%-NF-xy	0.42	0.84[†]	0.94	-0.01	2891[†]	447[†]	0.68	0.77	0.78	-0.02	2502	456	0.13
D2 180%	D2-180%-S1-xy*	0.58	0.85	1.01	-	2885	463	0.93	1.20	2.38	-	4022	674	0.12
	D2-180%-FF-x[2]	0.98	1.23	2.43	-0.01	4477	705	0.08	0.13	0.09	-0.02	534	97	0.11
	D2-180%-FF-y	0.06	0.16	0.12	-0.01	803	153	0.99	1.18	2.02	-0.02	3713	607	0.19
	D2-100%-L-xy	0.51	0.77	1.16	-0.01	2771	451	0.53	0.77	0.99	-0.01	2482	425	0.31
	D2-180%-L-x[3]	0.97	1.06	2.04	0.00	3822	597	0.04	0.07	0.20	-0.02	230	44	0.18
D3	D3-100%-xy	0.38	0.92	2.16	-0.04	3435	548	0.47	0.79	1.22	-0.02	2549	466	0.87
	D3-120%-xy	0.50	1.09	2.65	-0.03	3987	612	0.65	1.03	2.72	-0.03	3675	632	0.51
	D3-150%-x	0.72	1.21	3.33	-0.02	4225	648	0.06	0.18	0.10	-0.03	622	117	0.09

Notes: Test labels follow a format of 'Design'-'Intensity'-'GM'-'Direction', e.g. Test 10 = D1a-100%-NF-xy

PGA = peak ground acceleration, PRA = peak roof (centre) acceleration, $d_{max,r}$ = peak roof drift, $d_{res,r}$ = residual roof drift, M_b = building peak base moment, V_b = building peak base shear, θ = building peak in-plane torsional rotation.

** Test was not fully completed due to the table shutting down after reaching the overturning limit.*

[†] The centre roof accelerometer (B2) was compromised so the A2 accelerometer location was used.

Peak lateral drifts during the D1a-25% tests were 0.08% and 0.12% in the EW and NS directions, respectively, and these increased to 0.14% and 0.44% during the D1a-50% tests. These drifts highlight the relatively stiff response of the building

during serviceability level earthquake demands and no significant damage or residual drifts were observed. During D1a-100% design level intensity tests the building reached peak lateral drifts of 0.63% and 1.06% in the EW and NS directions respectively during the Kobe unidirectional ground motion tests and 0.47% and 0.81% during the Loma Prieta bi-directional test. The EW direction drifts were comfortably below the 1.0% design level drift but the peak drift slightly exceeded the design drift in the NS direction of the building. Given that the design implemented strength reduction factors, the actual lateral strength of the building should result in measured drifts below the design target drift, as occurred in the EW direction. The higher drift demands in the NS direction were attributed to two factors: 1) The isolated wall-to-floor connection used in the NS direction of the building resulted in a lower overstrength due to the floor slab interaction when compared to the flexible wall-to-floor connection used in the EW direction of the building; 2) Videos of the slotted beam connections revealed that some of the steel fuse dissipaters in the NS direction frames had become loose during testing, leading to a small "dead-zone" in their response before engaging. The loose nuts on the fuse connections were discovered during removal after the entire D1a test series and it was estimated that a 1-2 mm gap may have developed preventing the fuse from being fully engaged during small cycles. It was concluded that the fuse nuts in the NS direction of the building may have started to loosen during initial white noise and ground motion iterations, where a large number of repeated motions were required to adjust table control settings for this loading direction. If the steel fuse connections had been discovered and retightened prior to the start of testing it is expected that lower drifts would have been achieved in the NS direction for all D1a tests.

During the D2-100% design level intensity tests the building reached peak lateral drifts of 1.29% and 1.22% in the EW and NS directions respectively during the Kobe ground motion tests and 0.94% and 0.78% during the Loma Prieta test. These drifts were comfortably below the 2.0% design level drift for the D2 building configuration and the similar peak drifts in each direction showed that the issues with the loose steel fuse connections encountered during the D1a tests was no longer a factor. The near fault Loma Prieta record consistently resulted in lower lateral drift demands compared to the far field Kobe record, highlighting that the building design was not sensitive to high velocity or pulse ground motion characteristics. When subjected to MCE demands (D2-180%) the building reached peak lateral drifts of 2.38% in NS directions during the Loma Prieta test (D2-180%-S1-xy) where the table shutdown prior to the full ground motion completing. During unidirectional MCE demands (D2-180%-FF) the building reached peak lateral drifts of 2.43% and 2.02% in the EW and NS directions, respectively. As expected, the MCE earthquake intensity resulted in minor spalling at the corners of all of the PT walls which was considered primarily cosmetic, and isolated cracking was also observed at the slotted beam joints and floor integrally connected to walls 1 and 3. Following the initial MCE tests a long-duration ground motion was also applied, initially bi-directionally at a reduced scale and then in just the EW building direction at full MCE spectral demands. During the long-duration tests the PT walls were subjected to a total of 12 cycles to lateral drifts greater that 1.0%. The D2-180%-L-x test was also repeated three times due to scale and DAQ issues without any accumulated damage or fatigue failures. After the entire MCE sequence (8 separate motions) the building was still in an acceptable condition and none of the steel fuse dissipaters were observed to have fractured.

The final D3 building configuration involved removing all of the energy dissipating devices and relying solely on the PT walls for lateral load capacity. During these D3 tests the lateral drifts reached 2.16% in the EW direction for 100% intensity, below the calculated design drift of 3.0% for this building configuration. When the ground motion was increased to 120% the building achieved a lateral drift of 2.72% in the NS direction, and at an intensity of 150% the building achieved a lateral drift of 3.33% in the EW direction. Spalling at the wall toes, minor cracking and spalling of the slotted beam joints, and cracking of the floors adjacent to walls 1 and 3 were observed at the conclusion of testing, but there was no significant loss of structural integrity.

The residual drifts were consistently low throughout the entire test sequence. D1a had the highest contribution to lateral capacity from hysteretic steel fuse dissipaters and did not record a measurable residual drift despite Walls A and C in the NS direction exceeding the moment ratio requirement to achieve static self-centering. This finding confirms that self-cenerting design requirements may be conservative as they ignore the dynamic shakedown as the earthquake motion diminishes, as highlighted by previous analytical research [39].

Lateral-load Response

Representative base moment-drift responses for building configurations D1a, D2 and D3 are plotted in Figure 8 based on the calculated inertia forces from the central floor accelerometers processed with a 45 Hz low-pass filter. The response to 25% intensity earthquake resulted in an essentially elastic response with minimal wall uplift. During the 50% earthquake intensity, the response clearly exceeds the wall decompression point with a non-linear response observed and noticeable hysteretic energy dissipation as the steel fuses are engaged. A slight softening can be observed in the NS direction for the D1a-50% test, likely as a result of damage to the shims used in the isolated wall-to-floor connection (discussed in subsequent sections). The D1a-100% test response followed a flag-shaped response characteristic of post-tensioned wall

systems with additional energy dissipating devices. Interestingly the EW direction had slightly larger residual drifts in the hysteresis loops with an offset in the unloading and reloading response compared to the more ideal pinched response of the NS direction, despite the NS direction having a greater portion of the design flexural capacity attributed to the hysteretic energy dissipating components. This behaviour was attributed to the wall-to-floor connections, with the flexible slabs in the EW direction unintentionally contributing to hysteretic response whereas the isolated connections in the NS direction had little impact on the hysteretic response. The design base moment capacity (M_n) was exceeded during the D1a-100% tests in both the NS and EW loading directions.

The D2 building response also followed a characteristic flag-shaped response due to the greater portion of lateral capacity derived from the self-centering PT walls compared to the D1a design. As with the D1a response, the EW direction hysteresis loops had a noticeable offset in the unloading and reloading response due to the influence of the flexible wall-to-floor connections. The D2 building also comfortably exceeded the design base moment capacity at drifts well below the 2% design drift. The D3 building response followed a more non-linear elastic response that is characteristic of PT walls with no additional energy dissipating components. The larger drift cycles experienced more significant hysteresis due to minor spalling of the wall toes, small losses in wall PT force, and cracking of the flexible floor slab connections.

The design base moment capacity was comfortably exceeded for all building designs and loading directions. The system overstrength was more pronounced in the EW direction, with the D2 building exhibiting a measured base moment capacity at the 2% design drift approximately 50% larger than the design capacity in the EW direction compared to a 25% overstrength in the NS direction. This larger overstrength in the EW direction was attributed to the additional capacity as a result of the interaction between the walls and floor. However, it should be noted that the additional overstrength was controlled by using a flexible link slab, which greatly improved the performance and reduced the overstrength relative to the prior building tested at E-defense where a stiffer wall-to-floor connection was used [26].

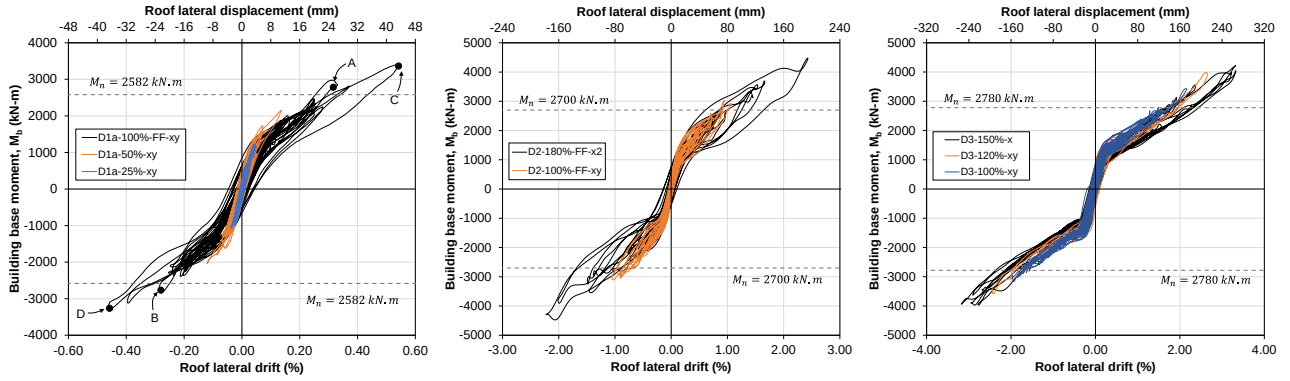

(a) EW direction

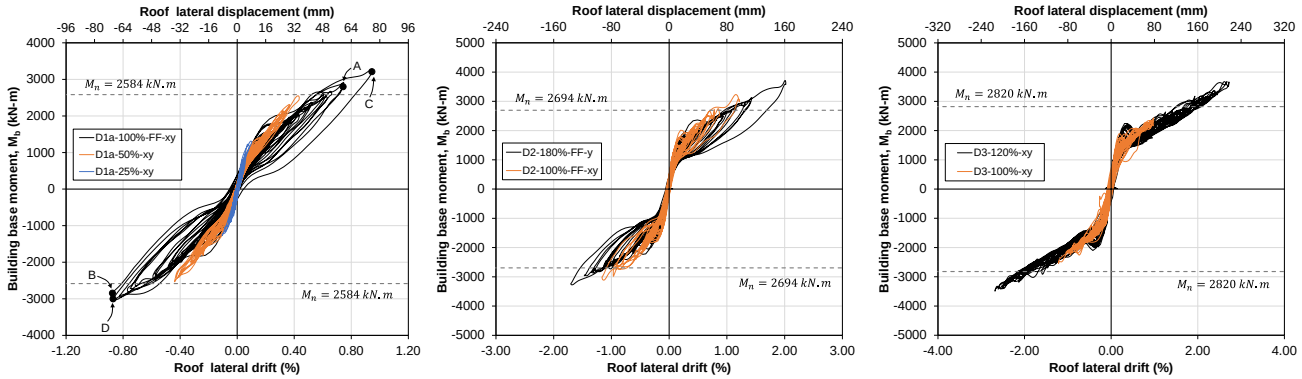

(b) NS direction

Figure 8 Lateral-load response for D2 and D3

First Mode Period

The first mode translational period of the building in both directions was calculated from white noise tests conducted before and after each series of tests. The acceleration data from all eight accelerometers on the two floors were subjected to a

frequency domain-based algorithm, enhanced frequency domain decomposition, to identify the structural period at both directions of the building. The calculated period estimates are plotted in Figure 9. The measured period in the EW direction at the start of testing was 0.21s, approximately equivalent to analytical estimates using $0.5I_g$ for the PT walls which is similar to recommendations from previous post-tensioned wall testing [13]. The measured period in the EW direction was relatively stable throughout the entire test sequence, with a period of 0.22s at the conclusion of the D2 building tests, an increase of only 6% from the start of testing. The increased damage caused during the D3 building tests resulted in a final period in the EW direction of 0.26s equal to a 24% increase from the start of testing. It should be noted that a 24% period lengthening is extremely small relative to that observed in conventional RC walls and a significant improvement on the PT wall building previously tested at E-defense[26] that exhibited a 30% period lengthening after 50% intensity tests (drift demands of ~0.65%) and an 88% period lengthening after the 100% design level intensity tests (drift demands of ~2.1%). These results highlight the improvement in damage control for the test building due to explicit consideration of wall-to-floor interaction and successful wall base detailing.

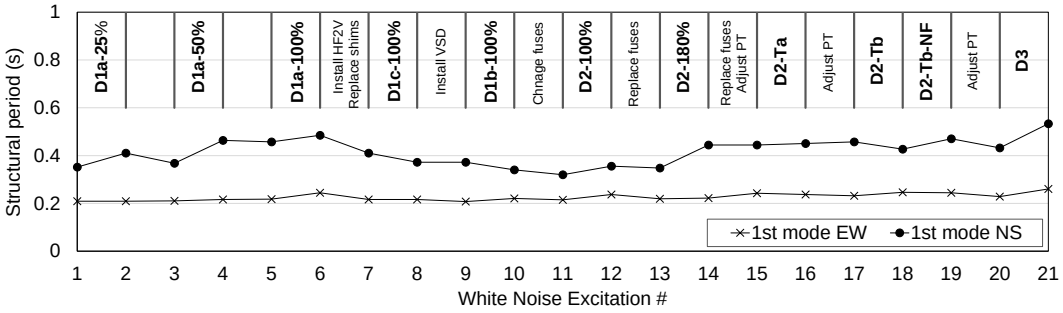

Figure 9 Variation in period throughout tests

The measured period in the NS direction at the start of testing was 0.35s, which is larger than analytical estimates using $0.5I_g$ for the PT walls. In addition, the period in the NS direction fluctuated significantly throughout the test sequence, reaching 0.48s (38% increase) after the D1a tests, dropping to 0.32s (9% decrease) after reconfiguring to D2, increasing to 0.44s (26% increase) after the D2 tests, and ending at 0.53s (52% increase) at the conclusion of D3 tests. The observed damage to walls A and C in the NS direction was typically less than the damage to damage to walls 1 and 3 in the EW direction due to the different armouring details used, implying that the period fluctuations were not exclusively related to the building damage. Instead it was concluded that detailing of the isolated wall-to-floor connections in the NS direction contributed to the period fluctuations. The isolated connection was originally designed with a 1-2mm gap between the tongue and the plastic shims and this gap influenced the dynamic characteristics of the building. In addition, throughout the D1a tests the plastic shims became scuffed and squashed, further increasing the gap or slop in the connection. The shims were periodically replaced between test series (as noted in Figure 9) and the initial gap was reduced where possible, resulting in reduction in the measured period at the start of new test series. While the final period in the NS direction was still a respectable 52% increase from the start of testing, an improvement to the detailing of the isolated connection and use of shims with a higher toughness would result in a substantial improvement in maintaining the building initial stiffness.

Post-tensioned Walls

The post-tensioned walls were designed to uplift and rock at the wall-to-foundation joint, with specific base detailing and armouring to prevent sliding and crushing in the highly stressed compression toes. The walls in both directions uplifted cleanly from the base pockets with combined in-plane and out-of-plane rotation when subjected to bi-directional ground motions. Photos showing the condition of representative walls at the conclusion of each test series are shown in Figure 10. There was no significant damage to Walls 1 and 3 (EW direction) during the entire D1a test series. The wall separated cleanly from the grouted pocket, with only minor debris (<5 mm) as the wall armouring separated from the grout. For the more heavily armoured Walls A and C (NS direction), some minor spalling was observed at the top of the stiff armouring plates, the most significant of which occurred to the North end of Wall A where the spalling extended ~140 mm along the wall length with a depth of only 5 mm.

For Walls 1 and 3 the spalling gradually progressed with increasing ground motion intensity or drift demands, with the loss of the cover on the end faces during D2-100% ground motions and with spalling extending 100-300 mm along the length of the walls and a maximum of 150 mm up the wall height. No significant crushing of the confined core concrete was observed. For Walls A and C the extent of spalling at the North end of Wall A did not increase from D1a through to the conclusion of testing (see Figure 10), and the spalling of other wall ends was similar at the conclusions of testing extending a maximum of 230 mm along the length of the wall and a maximum of 80 mm up the wall height.

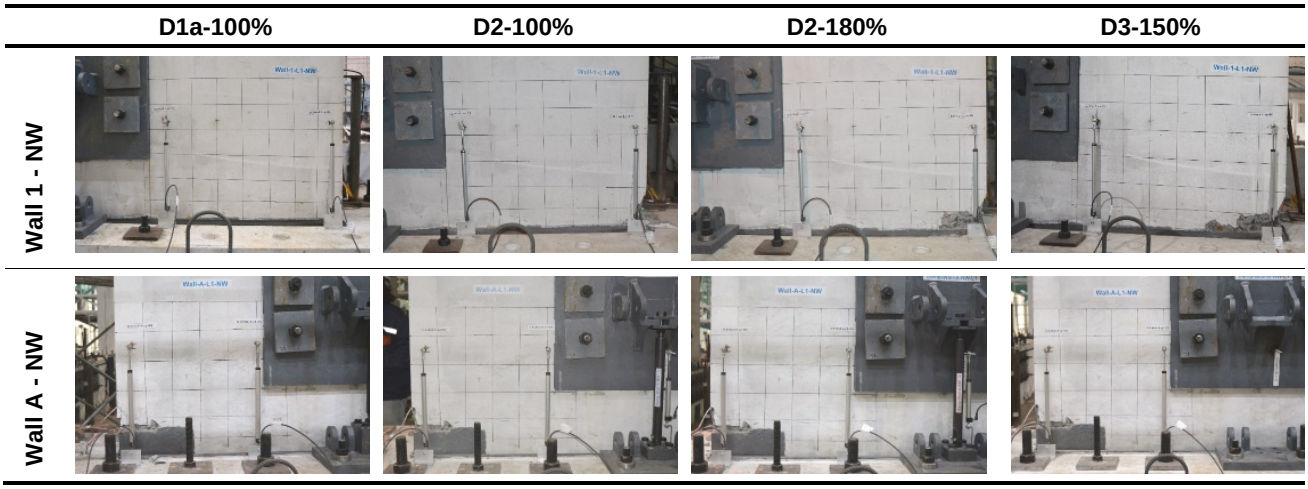

Figure 10 Wall Base Damage Progression

No significant in-plane or out-of-plane slip occurred for any of the walls. The grouted pocket detail and light armouring angle used for Walls 1 and 3 proved successful with no damage during lower drift tests. This result is an improvement on the details used in prior tests where the grout layer was positioned above the foundation surface and experienced some crushing [26, 28]. Notably, this connection also relied primarily on friction for shear transfer at the wall-to-foundation joint, with no shear dowels and with the grout only extending ~5 mm above the base of the wall. The heavier Wall A and C armouring detail was successful at reducing the extent of spalling during larger drift demands, with less damage observed compared to Walls 1 and 3.

Table 5 Peak wall response parameters

Test		Wall 1 Drift to East						Wall A Drift to North					
		$d_{max,r}$ (%)	θ_w (%)	c (mm)	ε_c (m/m)	Δ_u (mm)	f_p (%f_y)	$d_{max,r}$ (%)	θ_w (%)	c (mm)	ε_c (m/m)	Δ_u (mm)	f_p (%f_y)
D1a 25%	D1a-25%-x[2]	0.08	0.04	620	-0.0005	1.0	65						
	D1a-25%-y							0.10	0.05	429	-0.0004	0.9	44
	D1a-25%-xy	0.05	0.01	728	-0.0003	0.3	64	0.10	0.04	434	-0.0004	0.8	44
D1a 50%	D1a-50%-x	0.10	0.06	611	-0.0006	1.2	65						
	D1a-50%-y							0.41	0.34	225	-0.0014	6.2	49
	D1a-50%-xy	0.15	0.11	466	-0.0009	2.4	66	0.43	0.35	219	-0.0014	6.4	49
D1a 100%	D1a-100%-FF-x[2]	0.63	0.56	220	-0.0023	13.1	76						
	D1a-100%-FF-y							0.98	0.89	157	-0.0026	16.6	59
	D1a-100%-FF-xy	0.55	0.47	254	-0.0022	10.8	74	0.96	0.88	161	-0.0028	16.4	59
	D1a-100%-NF-xy[3]	0.48	0.42	271	-0.0021	9.6	72	0.75	0.66	179	-0.0022	12.2	54
D2 100%	D2-100%-FF-x[2]	1.28	1.17	179	-0.0043	27.5	65						
	D2-100%-FF-y[2]							1.15	1.02	168	-0.0032	18.9	58
	D2-100%-FF-xy	1.06	0.95	202	-0.0040	22.2	60	1.14	1.00	176	-0.0033	18.4	58
	D2-100%-NF-xy	0.96	0.88	208	-0.0039	20.3	58	0.85	0.72	196	-0.0026	13.3	53
D2 180%	D2-180%-S1-xy	0.98	0.89	210	-0.0035	20.6	57	2.14	1.94	147	-0.0057	36.2	73
	D2-180%-FF-x[2]	2.44	2.27	161	-0.0081	53.3	87						
	D2-180%-FF-y							2.01	1.83	152	-0.0055	34.1	71
	D2-100%-L-xy	1.04	0.93	233	-0.0048	21.4	56	0.77	0.65	222	-0.0030	11.8	49
	D2-180%-L-x[3]	1.78	1.63	180	-0.0065	38.2	71						
D3	D3-100%-xy	2.29	2.13	179	-0.0087	49.9	85	1.29	1.20	159	[no data]	22.5	61
	D3-120%-xy	2.75	2.59	181	-0.0111	60.5	94	2.67	2.48	140	-0.0071	46.7	82
	D3-150%-x	3.33	3.12	178	-0.0137	72.8	99						

Notes: $d_{max,r}$ = peak roof drift of the corresponding grid of the wall, θ_w = wall base rotation at the peak drift, c = average compression depth at end of wall at the peak drift, ε_c = average compressive strain at the end of the wall at the peak drift, Δ_u = average uplift at end of the wall at peak drift, f_p = PT stress at peak drift as a % of PT yield stress (average values when using multiple PT bars)

Wall response parameters measured at peak drifts for each test are summarised in Table 5 including base rotation, compression depth, compression strains, uplift, and PT force. Wall lateral deformations were primarily due to base rotation or rocking, accounting for between 90-95% of the lateral deformation during large drift tests. Compression depths and strains were sensitive to bi-directional demands when combined in-plane and out-of-plane rocking occurred, with average compression depths at peak drifts aligning well with design values. The compression strains were measured over a height of ~360 mm ($2.4t_w$), with peak strains below 0.003 m/m for all D1a tests and strains in excess of 0.010 m/m during the D3 tests when the largest building drifts were achieved.

The wall PT bars displayed typical trends during tests with the force increasing as the wall uplifted during lateral drifts, as shown by the examples plotted in Figure 11. For most tests the PT bars followed a linear response as the wall uplifted with no significant prestress loss occurring (see Figure 11a). As summarised in Table 5, the PT bar stresses in Walls A and C remained below $0.9f_y$ for all tests, whereas the Wall 1 and 3 average PT bar stresses reached close to $0.9f_y$ during D2-180% tests and close to $1.0f_y$ during the final D3-150% test. Noticeable yielding of the Wall 1 PT bars during the D3-150%-x is visible in Figure 11b, resulting in a partial loss of initial PT force. The variation in initial PT stress for Wall A throughout the entire test sequence is plotted in Figure 12. The Wall A PT bars were stressed slightly above the target stress during D1a and remained consistent through the test series with no significant prestress loss. The Wall A PT bars were stressed to the new target at the start of the D2 tests and experienced some minor prestress loss during D2-100% tests dropping to 98% of the target initial stress. During the D2-180% tests the Wall A bars experienced some additional prestress loss, ending at 95% of the target initial stress. The PT bars were restressed prior to the D3 tests, where they again experienced some minor prestress loss due to yielding.

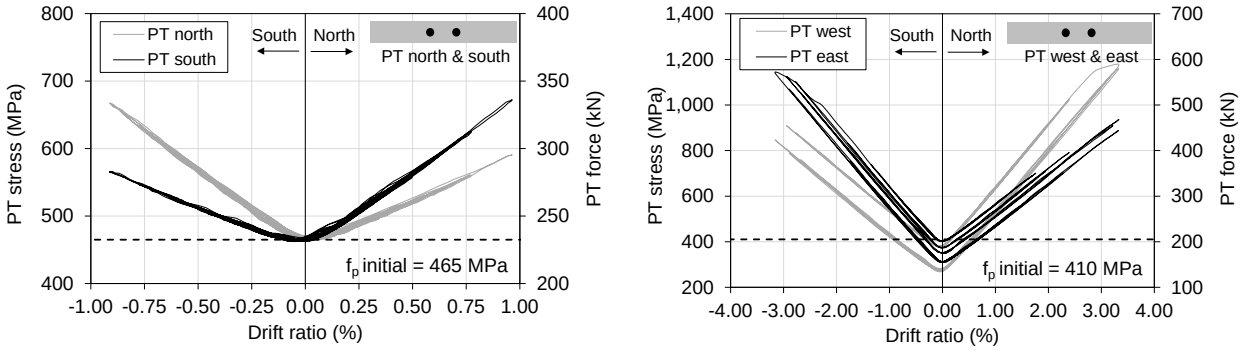

(a) Wall A test D1a-100%-xy

(b) Wall 1 test D3-150%-x

Figure 11 Measured PT bar forces

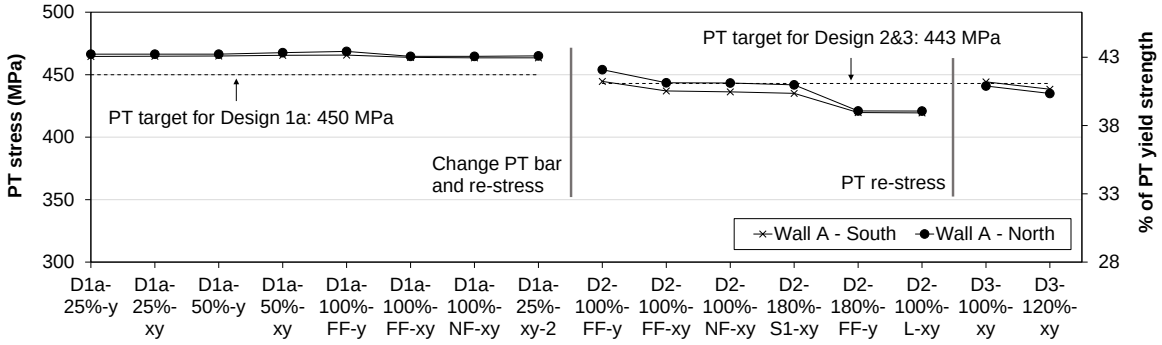

Figure 12 Variation of initial PT stress during testing

Frames

The frames performed well during the tests, with rocking at the column base and opening and closing of the slotted beam joints. With the exception of some flexural cracks in the Grid A and C beams due to gravity demands, there was no significant seismic cracking or damage to either the beams or columns. The slotted beam joints opened and closed cleanly, allowing the energy dissipating devices used in the D1a building design to yield in tension and compression. The deformation profiles measured across the beam joint showed the joint rotating about the top hinge, with axial elongation

at the floor level approximately 1-2 mm max, significantly less that the corresponding elongation observed in conventionally reinforced beams that is attributed to high levels of damage to floors[40]. No significant vertical shear slip or torsional rotation were measured at the most highly loaded Grid A and C beam joints, indicating that the design of the diagonal hanger reinforcement was adequate to provide load transfer at the ends of the beams. During the D1a tests, there was evidence of the beam pivoting about the top with a narrow crack observed at the beam-column interface. Following the D2-100% tests the beams were still essentially undamaged, with only minor spalling at the top of a couple of the beam joints, as shown in Figure 13a. At the conclusions of testing there was localised spalling observed at the top of most joints, as shown in Figure 13Figure 13b. The columns were essentially undamaged throughout the entire test sequence, with only very minor chipping of concrete (<5 mm deep) directly above the steel armouring angles which occurred during the D3 building tests, as shown in Figure 13Figure 13c.

(a) Beam 3@C-L1 after D2-100% (b) Beam 3@C-L1 after D3-150% (c) Col A1 after D3-150%

Figure 13 Beam and column damage

Floor Interaction and Response

The test building was explicitly designed with details that addressed deformation compatibility between structural components, including wall-to-floor connections that were intended to minimise floor damage and second order structural actions. The flexible wall-to-floor connections in the EW or longitudinal direction allowed the wall uplift and rotation to be accommodated while maintaining an integral connection and stiff in-plane load path for lateral load transfer. The Level 1 out-of-plane floor deformations measured at the peak drift of a D2-180% test are plotted in Figure 14. The peak out-of-plane floor deformation at the end of the wall closely matched the uplift at the wall base. This vertical deformation was primarily accommodated within the flexible link slab, as was intended by design, with the out-of-plane deformation at the edge of the double tee (line 1i) similar to the center of the floor (line 2). It should be noted that the entire floor displaced vertically at the center by 5-10 mm due to the columns supporting the floor also uplifting as they rocked as well as vertical vibration of the floor. The Level 2 floor performed in a similar manner to Level 1, except that the out-of-plane deformations were accommodated by the flexible composite floor spanning between the wall on grid 1 and the steel beam on grid 2.

The isolated wall-to-floor connections in the NS or transverse direction allowed the wall uplift and rotation to occur independently from the floor while maintaining in-plane lateral load transfer. The measured vertical tongue-to-wall displacement confirmed that sliding of the tongue within the wall slot occurred as the wall uplifted in a similar pattern to the wall base uplift. The measured tongue-to-wall horizontal displacements showed that a small displacement was required prior to the tongue engaging with the side of the slot. As noted earlier there was a 1-2 mm gap between the tongue and the shims and this initial gap aligns well with the total rattle or slop measured between the tongue and wall of ~2-3 mm. Although the isolated connection worked as intended with vertical sliding of the tongue within the slot, the repeated movement caused damage to the plastic shims that were installed to accommodate the construction tolerances. As the test series progressed the shims became squashed and bent, resulting in an increase in the gap between tongue and shim. The shims were replaced at several points throughout the test sequence when visible damage was observed. Although the shim damage was primarily attributed to the large number of repeated tests, use of a tougher shim material may result in an improved connection response.

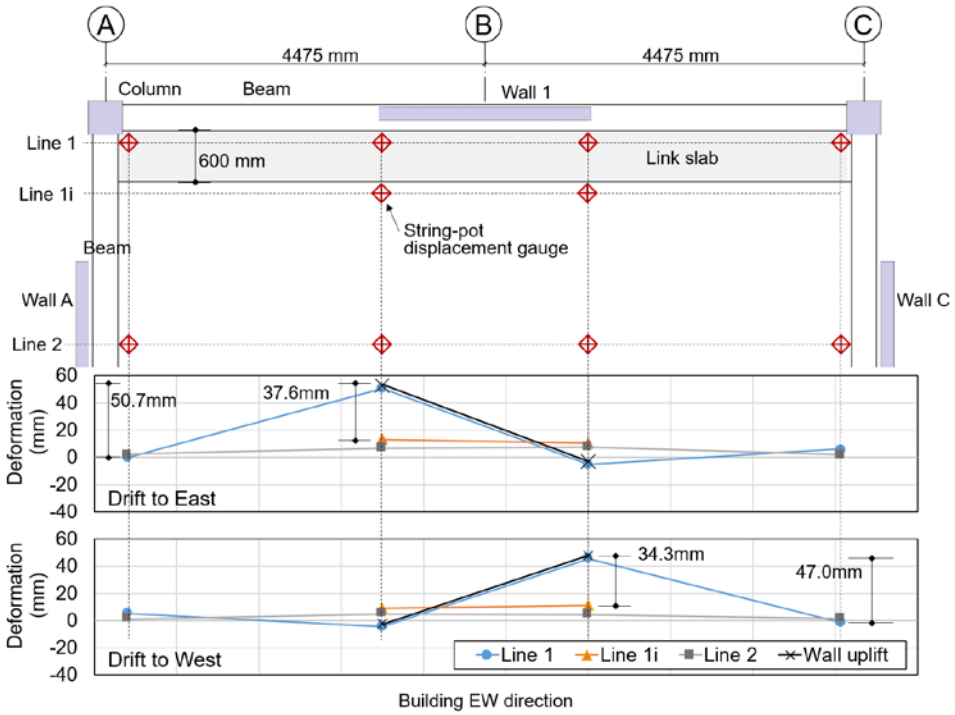

Figure 14 Level 1 out-of-plane floor deflections at peak drift for test D2-180%-FF-x[2]

The mapped crack patterns on the top of both floors at the conclusion of testing are illustrated in Figure 15 and the residual crack widths at the conclusions of each series of tests are summarised in Table 6. For the Level 1 floor the cracking was almost entirely contained within the flexible link slabs. The distributed cracking in the link slab occurred as it accommodated the vertical deformations of the wall and connected beams while the double tees remained stiff and undamaged. On the Level 2 floor the cracking was concentrated in the region adjacent to Walls 1 and 3 and extended into the center of the floor. Although the cracking looks significant in the illustrations, the crack widths were typically narrow, as is highlighted by the photo in Figure 16 that shows the damage adjacent to Wall 3 at the end of testing. At the end of the D1a testing, the largest residual crack width was only 0.4 mm with most cracks less than 0.2 mm wide. At the end of the D2-100% testing, the largest residual crack width was only 0.5 mm at the wall-to-floor interface, with most cracking within the link slab and floor 0.2 mm in width or less. The crack widths continued to widen during repeated large intensity shaking during the D2-180% and D3 tests, with residual crack widths of up to 1.2 mm at the conclusion of testing. The final residual crack widths are considered to be an excellent result for a building that was subjected to a large number of high intensity earthquakes and detailing of the wall-to-floor and floor-to-beam connections was successful at minimising damage due to component interactions.

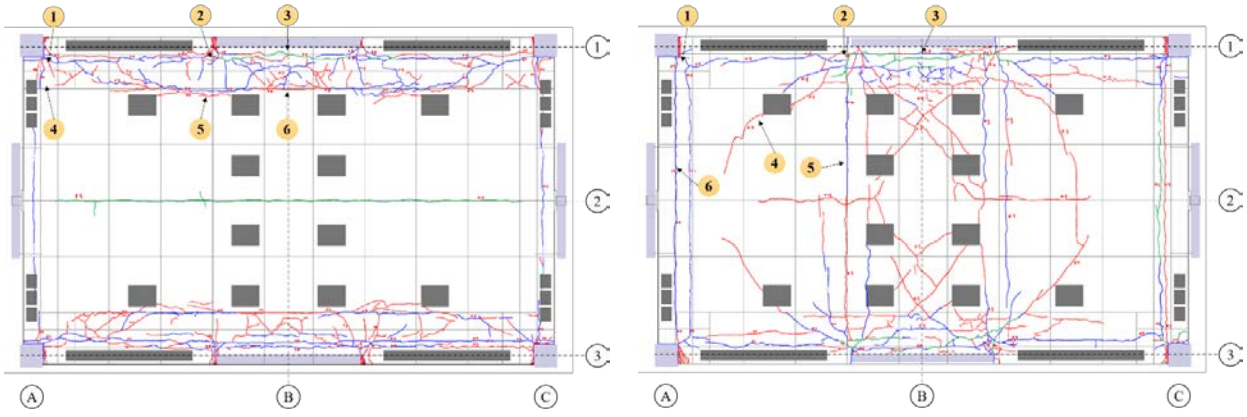

(a) Level 1 (b) Level 2

Figure 15 Floor crack pattern at end of testing

Table 6 Floor residual crack widths (mm)

Level	No.#	Location	D1a-25%	D1a-50%	D1a-100%	D2-100%	D2-180%	D3-150%
Level 1	①	Link slab - Beam interface at column end	N/A	0.2	0.2	0.3	0.3	0.3
	②	Link slab - Beam interface at wall end	0.2	0.2	0.3	0.4	0.6	1.0
	③	Link slab - Beam interface at wall center	0.2	0.3	0.3	0.5	1.0	1.2
	④	Link slab - Double tee interface at column end	N/A	N/A	N/A	0.1	0.1	0.1
	⑤	Link slab - Double tee interface at wall end	N/A	N/A	0.1	0.2	0.3	0.4
	⑥	Link slab - Double tee interface at center	N/A	N/A	N/A	N/A	0.5	0.6
Level 2	①	Longitudinal beam - Floor interface at column end	N/A	N/A	0.2	0.2	0.3	0.2
	②	Longitudinal beam - Floor interface at wall end	0.2	0.2	0.3	0.4	0.6	1.0
	③	Longitudinal beam - Floor interface at wall center	0.1	0.2	0.4	0.5	0.8	1.0
	④	Transverse beam - Floor interface at wall center	0.1	0.1	0.1	0.3	0.3	0.4
	⑤	Perpendicular to end of wall	0.2	0.2	0.2	0.3	0.3	0.4
	⑥	Diagonal crack from wall end to mid of transverse beam	N/A	0.2	0.2	0.2	0.3	0.2

 # Crack numbers shown on the floor illustrations in Figure 15.

Figure 16 Floor damage adjacent to Wall 3 on Level 1

REPAIRABILITY

The test building was explicitly designed to meet an enhanced performance level targeting immediate occupancy following earthquakes. A summary of key structural response and damage parameters at the conclusion of each series of tests is provided in Table 7. Residual drifts were essentially zero throughout the entire test series and well below acceptable residual drift limits. The maximum loss of wall PT force was ~10% during 180% intensity ground motion tests and this was considered to be acceptable and would not necessarily require restressing in a real building. As noted earlier the initial building stiffness/period was relatively stable in the EW direction, with a maximum increase in period of 24% during the D3 tests. In the NS direction the stiffness was affected by the initial gap and subsequent damage to the shims in the isolated wall-to-floor connections. Although the maximum increase in period of 52% would likely still be acceptable for the building to meet serviceability requirements, an improvement in the shim design could improve this outcome and minimise the need to replace the shims. Overall, the building maintained a lateral strength that exceeded the design strength with no measurable loss in structural integrity. Based on the building response it was concluded that repairs were not likely to be required to recover any lost structural capacity.

Component damage was typically concluded to be minor and cosmetic. For the walls minor spalling initiated during 100% intensity tests and moderate spalling occurred during 180% intensity tests. It should be noted that moderate spalling relates to significant loss of cover concrete to the depth of the confinement reinforcement which has no significant impact on the wall strength and requires only cosmetic repairs to reinstate the cover. Cover concrete patch repairs would also be essential to maintain durability requirements for external walls. The beam damage was minor for most tests and only during the final D3 tests did noticeable spalling occur at the top of the beam slot. Again, this spalling did not compromise the beam shear or torsional strength and so a minor cosmetic repair would be required. Cracking in the floors was distributed and with the exception of the primary crack at the wall-to-floor interface, with most cracks no wider than 0.2 mm. Many of the cracks are no wider than typical shrinkage cracks observed in an existing building, so it is concluded that no repairs would be required. However, epoxy injection repair of the widest cracks (~1.0-1.2 mm) may be likely following the 180% intensity ground motion tests.

Table 7 Low-damage response parameters

			D1a-25%	D1a-100%	D2-100%	D2-180%	D3-150%
Structural response	**Residual drift (%)***		0.00%	0.01%	0.02%	0.02%	0.03%
	Residual PT stress	**NS**	103%	103%	99%	95%	95%
	(% of target)*	**EW**	102%	101%	99%	90%	70%
	Increase in period (%)	**NS**	17%	38%	1%	26%	52%
		EW	0%	17%	13%	6%	24%
	Residual lateral strength		>100%	>100%	>100%	>100%	>100%
	(% of design strength)						
Damage	**Wall spalling**	**1/3***	None	None	Minor	Moderate	Moderate
		A/C*	None	Minor	Minor	Minor	Moderate
	Beam spalling*		None	None	Minor	Minor	Moderate
	Column spalling*		None	None	None	None	Minor
	Floor cracks	**Max**	0.2 mm	0.4 mm	0.5 mm	1.0 mm	1.2 mm
		Typical	<0.1 mm	<0.2 mm	0.2 mm	0.2 mm	0.2 mm
Repair outcome#			No repair	No repair	No repair	Minor / cosmetic repair	Minor / cosmetic repair

** Reported for the worst building direction or component*
 # Excluded replacement of energy dissipating devices and shims in isolated wall connections

Overall, the building was deemed to have met the performance objectives with immediate occupancy achieved for all tests and only minor cosmetic repairs required after the 180% intensity maximum consider earthquake demands. This is a remarkable achievement and a significant improvement on the outcome of other comparable test buildings that used PT walls [26, 28]. It is concluded that a combination of post-tensioned walls and slotted beams can provide an excellent low-damage structural system if designed and detailed appropriately.

SYSTEM RESILIENCE

The low-damage test building was also shown to have excellent resilience beyond the design performance objectives. The structural systems and connection detailing used in the test building were able to satisfy the enhanced damage control design objectives while also substantially exceeding life-safety design requirements. The resilience of the test building was demonstrated in a number of ways:

- The D2 building configuration was subjected to five separate tests at a maximum considered earthquake intensity equal to 180% of the design earthquake intensity with no loss of structural integrity and only repairable damage.
- The D2 building configuration was subjected to three repeated runs of test 29, a long-duration earthquake record at 180% intensity, with no loss of structural integrity or low-cycle fatigue failure of the steel fuse dissipaters.
- The PT walls are designed to prevent yielding of the PT bars at the design drift and with extensive confinement and armouring to prevent wall crushing failures. When designed according to current recommendations, the PT walls were shown to have substantial reserve strength and deformation capacity. The post-uplift stiffness of the PT walls helps to control drifts during earthquakes larger than design and the PT bars can be subjected to deformations well beyond the design limits.
- PT bar anchorages were found to be more resilient to repeated cyclic loading than PT strand anchorages that have failed at low strains during prior testing and require specialist anchor systems and carful installation when used in unbonded PT walls [41].
- The slotted beams behaved essentially as pinned connections when no energy dissipating devices were installed and had a large rotational capacity with no loss of structural integrity. The diagonal hanger reinforcement was sufficient to maintain shear and torsion strength throughout the entire test sequence. No significant residual axial elongation of slotted beam joint or frame dilation was observed.
- The floors systems and support connection detailing showed no indication of damage or movements that might compromise their support, a significant improvement on precast floor systems installed in conventional reinforced concrete buildings [40].
- The connection detailing was designed to have sufficient excess deformation compatibility. Movement allowances (e.g. beam slots, slotted wall-to-floor connection) were designed to accommodate drift demands in excess of twice that expected during maximum consider earthquake demands.

- Even when all energy dissipaters where removed during the building D3 tests, a satisfactory structural response was achieved with no loss of structural integrity when lateral drift demands exceeded 3.3%. The testing was only terminated after the D3-150% tests due to the table overturning capacity being exceeded.

CONCLUSIONS

The test programme and key results were presented for a shake table test of a 2-storey low-damage concrete wall building that implemented state-of-art design concepts and practical construction details. The test allowed for the building system response to be investigated when subjected to bi-directional shaking demands. Overall, the performance of the test building was excellent, with the reliable structural response and minimal damage demonstrating the advantages of the low-damage structural systems implemented. Key results were presented from which the following conclusions were drawn:

1. The direct displacement-based design method used for the test building was appropriate with peak drifts measured during testing all below the respective design drift targets, with the exception of the D1a building configuration NS direction. The unexpected large drift demands in the D1a NS direction were attributed to loose nuts on the steel fuse dissipaters that were not discovered until after testing was complete.

2. The building recentered with no significant residual drifts for all tests despite the design slightly exceeding current recentering recommendations derived from static equilibrium. This finding confirms that self-centering design requirements are conservative as they ignore the dynamic shakedown effect.

3. The measured base moment capacity was approximately 50% larger than the design capacity in the EW direction and 25% larger than the design capacity in the NS direction. The larger overstrength in the EW direction was attributed to the additional capacity from floor participation. However, it should be noted that the overstrength was controlled by using flexible link slab that greatly improved the performance when compared to stiffer wall-to-floor connections used in prior tests.

4. Damage to the wall base was limited to minor spalling in the toes, with some minor cracking and spalling of the beam joints and distributed cracking in the flexible floor connections. The lack of damage resulted in a reasonable stable initial stiffness in the EW direction with a maximum 24% period lengthening at the end of testing, much lower than the degradation observed in conventional RC walls and prior PT wall building tests. These results highlight the successful damage control for the test building due to explicit consideration of wall-to-floor interaction and successful wall base detailing.

5. The two alternative wall base details performed well with clean uplift of the wall and no significant in-plane or out-of-plane slip. The grouted pocket detail and light armouring angle used for Walls 1 and 3 was undamaged during lower drift tests and proved to be an improvement on the details used in prior tests where the grout layer positioned above the foundation surface experienced crushing. The heavier Wall A and C armouring detail was successful at reducing the extent of spalling during larger drift demands, with less damage observed compared to Walls 1 and 3.

6. The frames performed well during the tests, with rocking at the column base and opening and closing of the slotted beam joints with minimal damage. No significant vertical shear slip or torsional rotation were measured at the beam joints, confirming that the design of the diagonal hanger reinforcement was adequate to provide load transfer at the ends of the beams.

7. Both wall-to-floor connections successfully addressed deformation compatibility. For the flexible connections, vertical deformation was primarily accommodated within the link slab or composite floor span with well distributed narrow cracks forming. The isolated wall-to-floor connection successfully allowed the wall to uplift and rotate without imposing deformations or damage to the adjacent floor, but improved detailing could prevent shim damage and reduce the initial gap or rattle that influenced the initial stiffness and period in the NS direction of the building.

8. The building maintained lateral strength throughout testing with no measurable loss in structural integrity and it was concluded that repairs were not likely to be required to recover any lost structural capacity. Instead, a cosmetic repair would be implemented to reinstate the cover on spalled wall toes and beam joints, with possible epoxy injection of the widest floor cracks adjacent to Walls 1 and 3.

9. The building was deemed to have met the immediate occupancy performance objective for all tests including repeated 180% intensity maximum consider earthquake demands. This is a remarkable achievement and a significant improvement on the outcome of other comparable test buildings that used PT walls. It is concluded that a combination of post-tensioned walls and slotted beams can provide an excellent low-damage structural system if designed and detailed appropriately.

10. The low-damage structural system demonstrated a high degree of resilience, being subjected to a total of 39 separate tests, many of which were at a design level or maximum considered earthquake intensity. Both the post-tensioned walls and slotted beams had sufficient reserve strength and deformation capacity and the connection detailing provided allowance for large deformations without any loss of structural integrity.

DATA AVAILABILITY

A complete dataset of the test has been published on DesignSafe-CI [30]. The dataset contains details of the test building design and construction in addition to all test data including sensor data, photos, videos, inspection sheets, etc. Researchers are encouraged to access and use the dataset and reference the published dataset DOI.

ACKNOWLEDGEMENTS

The authors would like to acknowledge the funding provided by the International Joint Research Laboratory of Earthquake Engineering (ILEE) at Tongji University, the Building Systems Performance branch of the New Zealand Ministry of Business, Innovation and Employment (MBIE), the New Zealand Centre for Earthquake Resilience (QuakeCoRE), and ConcreteNZ. The authors also would like to acknowledge Shanghai City-Raise Construction Group for their extensive support during component construction and building demolition, Livable Building Technology Co. Ltd and Huanyu Building Engineering Material Co. Ltd for donating the grout, and Stahlton Engineered Concrete and ComFlor Building Systems for donating the floor systems. The advice and support from the project industry advisory group is also greatly appreciated, including Alistair Cattanach, Didier Pettinga, Tony Holden, Peter Smith, Des Bull, and Craig Muir. In addition, the assistance of the technicians in Tongji University lab during setup and testing is also sincerely appreciated, in particular Prof. Chengyu Yang and Dr Lu for their persistence to ensure accurate control of the shake table. Lastly, the assistance of Qun Yang and Song Ge during the test preparation, testing, and data processing is greatly appreciated. This is QuakeCoRE publication number 0554.

REFERENCES

1. Marquis F, Kim J J, Elwood K J, Chang S E. *Understanding post-earthquake decisions on multi-storey concrete buildings in Christchurch, New Zealand.* Bulletin of Earthquake Engineering, 2017; 15(2): 731-758.
2. Priestley M J N, Sritharan S S, Conley J R, Pampanin S. *Preliminary Results and Conclusions From the PRESSS Five-Story Precast Concrete Test Building.* PCI Journal, 1999; 44(6): 42-67.
3. Kurama Y C, Sritharan S, Fleischman R B, Restrepo J I, Henry R S, Cleland N M, Ghosh S K, Bonelli P. *Seismic-Resistant Precast Concrete Structures: State of the Art.* Journal of Structural Engineering (United States), 2018; 144(4).
4. Perez F J, Pessiki S, Sause R. *Experimental lateral load response of unbonded post-tensioned precast concrete walls.* ACI Structural Journal, 2013; 110(6): 1045-1055.
5. Nazari M, Sritharan S, Aaleti S. *Single precast concrete rocking walls as earthquake force-resisting elements.* Earthquake Engineering and Structural Dynamics, 2017; 46(5): 753-769.
6. Holden T, Restrepo J, Mander John B. *Seismic Performance of Precast Reinforced and Prestressed Concrete Walls.* Journal of Structural Engineering, 2003; 129(3): 286-296.
7. Restrepo J, Rahman A. *Seismic Performance of Self-Centering Structural Walls Incorporating Energy Dissipators.* Journal of Structural Engineering, 2007; 133(11): 1560-1570.
8. Kurama Y C. *Hybrid post-tensioned precast concrete walls for use in seismic regions.* PCI Journal, 2002; 47(5): 36-59.
9. Marriott D, Pampanin S, Bull D, Palermo A. *Dynamic testing of precast, post-tensioned rocking wall systems with alternative dissipating solutions.* Bulletin of the New Zealand Society for Earthquake Engineering, 2008; 41(2): 90-103.
10. Sritharan S, Aaleti S, Henry R S, Liu K-Y, Tsai K-C. *Precast concrete wall with end columns (PreWEC) for earthquake resistant design.* Earthquake Engineering & Structural Dynamics, 2015; 44(12): 2075-2092.

11. Twigden K M, Sritharan S, Henry R S. *Cyclic testing of unbonded post-tensioned concrete wall systems with and without supplemental damping.* Engineering Structures, 2017; 140: 406-420.
12. Nazari M, Sritharan S. *Dynamic Evaluation of PreWEC Systems with Varying Hysteretic Energy Dissipation.* Journal of Structural Engineering (United States), 2018; 144(10).
13. Twigden K M, Henry R S. *Shake table testing of unbonded post-tensioned concrete walls with and without additional energy dissipation.* Soil Dynamics and Earthquake Engineering, 2019; 119: 375-389.
14. NZS 3101:2006. *Concrete Structures Standard (Amendment 3)*. Wellington, New Zealand: Standards New Zealand: 2017
15. Pampanin S, Marriott D, Palermo A, New Zealand Concrete Society. *PRESSS design handbook*. Auckland, New Zealand: 2010
16. ACI ITG-5.1-07. *Acceptance Criteria for Special Unbonded Post-Tensioned Precast Structural Walls Based on Validation Testing and Commentary*. Farmington Hills, Michigan: American Concrete Institute: 2008
17. ACI ITG-5.2-09. *Requirement for Design of a Special Unbonded Post-Tensioned Precast Shear Satisfying ACI ITG-5.1 (ACI ITG-5.2-09) and Commentary*. Farmington Hills, Michigan: American Concrete Institute: 2009
18. ACI 318-08. *Building Code Requirements for Structural Concrete (ACI 318-08) and Commentary*. Farmington Hills, Michigan: American Concrete Institute: 2008
19. Englekirk R E. *Design-construction of the Paramount - A 39-story precast prestressed concrete apartment building.* PCI Journal, 2002; 47(4): 56-71.
20. Cattanach A, Pampanin S, *21st century precast: the detailing and manufacture of NZ's first multi-storey PRESSS-building*, in *New Zealand Society for Earthquake Engineering Conference*. 2008: Rotorua, New Zealand.
21. Pampanin S, Kam W-Y, Haverland G, Gardiner S, *Expectation meets reality: Seismic performance of posttensioned precast concrete Southern Cross Endoscopy building during the 22nd Feb 2011 Christchurch.*, in *New Zealand Concrete Industries Conference*. 2011: Rotorua, New Zealand.
22. Henry R S. *Implementation of low-damage concrete wall buildings and detailing for deformation compatibility*. in *2018 Concrete New Zealand Conference*. 2018. Hamilton.
23. Henry R S, Sritharan S, Ingham J M. *Finite element analysis of the PreWEC self-centering concrete wall system.* Engineering Structures, 2016; 115: 28-41.
24. Watkins J, Sritharan S, Henry R S. *An experimental investigation of a wall-to-floor connector for self-centering walls*. in *Proceedings of the Tenth U.S. National Conference on Earthquake Engineering*. 2014. Anchorage, Alaska.
25. Liu Q, French C W, Sritharan S. *Performance of a Precast Wall with End Columns RockingWall System with Precast Surrounding Structure.* ACI Structural Journal, 2020; 117(3): 103-116.
26. Gavridou S, Wallace J W, Nagae T, Matsumori T, Tahara K, Fukuyama K. *Shake-Table Test of a Full-Scale 4-Story Precast Concrete Building. I: Overview and Experimental Results.* Journal of Structural Engineering, 2017; 143(6).
27. Watkins J, Sritharan S, Nagae T, Henry R S. *Computational modelling of a four storey post-tensioned concrete building subjected to shake table testing.* Bulletin of the New Zealand Society for Earthquake Engineering, 2017; 50(4): 595-607.
28. Schoettler M J, Belleri A, Dichuan Z, Restrepo J I, Fleischman R B. *Preliminary results of the shake-table testing for the development of a diaphragm seismic design methodology.* PCI Journal, 2009; 54(1): 100-124.
29. Belleri A, Schoettler M J, Restrepo J I, Fleischman R B. *Dynamic behavior of rocking and hybrid cantilever walls in a precast concrete building.* ACI Structural Journal, 2014; 111(3): 661-671.
30. Henry R S, Lu Y, Zhou Y, Rodgers G W, Gu A, Yang Q. *Dataset on shake table test of a low-damage concrete wall building*. DesignSafe-CI: 2020. *DOI to be conformed.*
31. Priestley M J N, Calvi G M, Kowalsky M J, *Displacement-based design of structures*. 2007, Pavia: IUSS Press.
32. Muir C A, Bull D K, Pampanin S. *Preliminary observations from biaxial testing of a two-storey, two-by-one bay, reinforced concrete slotted beam superassembly.* Bulletin of the New Zealand Society for Earthquake Engineering, 2012; 45(3): 97-104.
33. Liu R, Palermo A. *Fuse-Type External Replaceable Dissipaters: Experimental Program and Numerical Modeling.* Journal of Structural Engineering, 2020; 146(5).
34. Rodgers G W, Solberg K M, Chase J G, Mander J B, Bradley B A, Dhakal R P, Li L. *Performance of a damage-protected beam-column subassembly utilizing external HF2V energy dissipation devices.* Earthquake Engineering and Structural Dynamics, 2008; 37(13): 1549-1564.
35. Golzar F G, Rodgers G W, Chase J G. *Design and Experimental Validation of a Re-centring Viscous Dissipater.* Structures, 2018; 13: 193-200.
36. Yeow T Z, Orumiyehei A, Sullivan T J, MacRae G A, Clifton G C, Elwood K J. *Seismic performance of steel friction connections considering direct-repair costs.* Bulletin of Earthquake Engineering, 2018; 16(12): 5963-5993.
37. FEMA P-695. *Federal Emergency Management Agency. Quantification of Building Seismic Performance Factors, FEMA*. Washington DC, USA: 2009
38. NZS 1170.5:2004. *Structural design actions - Part 5: Earthquake actions - New Zealand*. 2016

39. Henry R S, Sritharan S, Ingham J M. *Residual drift analyses of realistic self-centering concrete wall systems.* Earthquake and Structures, 2016; 10(2): 409-428.
40. Henry R S, Dizhur D, Elwood K J, Hare J, Brunsdon D. *DAMAGE TO CONCRETE BUILDINGS WITH PRECAST FLOORS DURING THE 2016 KAIKOURA EARTHQUAKE.* Bulletin of the New Zealand Society for Earthquake Engineering, 2017; 50(2): 174-186.
41. Walsh K Q, Draginis R L, Estes R M, Kurama Y C. *Effects of anchor wedge dimensional parameters on posttensioning strand performance.* PCI Journal, 2015: 63-83.